Comparison of FEM and SPH for Modeling a Crushable Foam Aircraft Arrestor Bed

Matthew Barsotti, M.S.

Protection Engineering Consultants, LLC

Abstract

Passenger aircraft can overrun the available runway area during takeoff and landing, creating accidents involving aircraft damage and loss of life. Crushable foam arrestor bed systems are often placed at runway ends to mitigate such overruns. As the aircraft tires roll through the bed, the material compaction dissipates energy, bringing the aircraft to a controlled stop.

A detailed two-year analysis was conducted for the TRB Airport Cooperative Research Program to develop improved arresting systems (Barsotti, et al., 2009). A major thrust of the effort was the development of validated numerical models for crushable arrestor bed materials and deformable aircraft tires.

Finite element models for the crushable material manifested several problems due to the unusual mode of deformation experienced, which included significant element skewing, heavy compaction (~90%), and high hourglass energies (~19%). Many meshing and hourglass mitigation strategies were attempted, but they produced only marginal improvement.

The Smoothed Particle Hydrodynamics (SPH) method was adopted as a replacement, and detailed performance comparisons of the FEM and SPH versions were made. Error convergence studies using mesh refinement were performed for 1-D, 2-D, and 3-D cases, culminating in the comparison of full tire & arrestor models for each formulation.

Overview of Problem

Arrestor Background

The current arrestor technology for civil aircraft utilizes a large bed of crushable material placed at the end of a runway. This arrestor concept is designated by the Federal Aviation Administration (FAA) as an Engineered Material Arresting System (EMAS) (FAA, 2005).

If an aircraft overrun occurs, its tires roll through the EMAS bed, compacting the material. The aircraft is slowed by the induced drag load, and the energy absorbed is proportional to the volume of material compacted (Figure 1) (Barsotti, 2008).

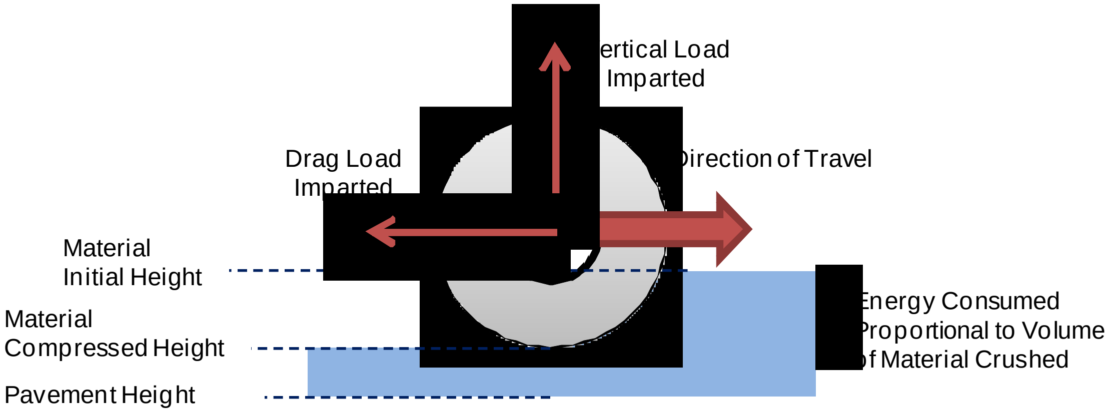

Figure 1. Arresting Performance of Crushable Materials

Idealized Material Assumptions

Only one variant of EMAS is current approved by the FAA, and it uses a cellular cement foam as the principal absorbent material (Barsotti, et al., 2009). However, other crushable foam materials are entirely viable. This research features a generalized foam material featuring the following assumptions:

- Crushable material with no elastic rebound
- Nominal compression strength of 50 psi
- Negligible Poisson's ratio
- Negligible rate effects
- Density roughly equivalent to current arrestor systems (18 – 25 pcf)
- Idealized step function profile for the compressive stress-strain curve
- High compressibility (85%)
- Negligible energy absorption in tension

Figure 2 shows a uniaxial compression curve for the idealized material (Barsotti, et al., 2009).

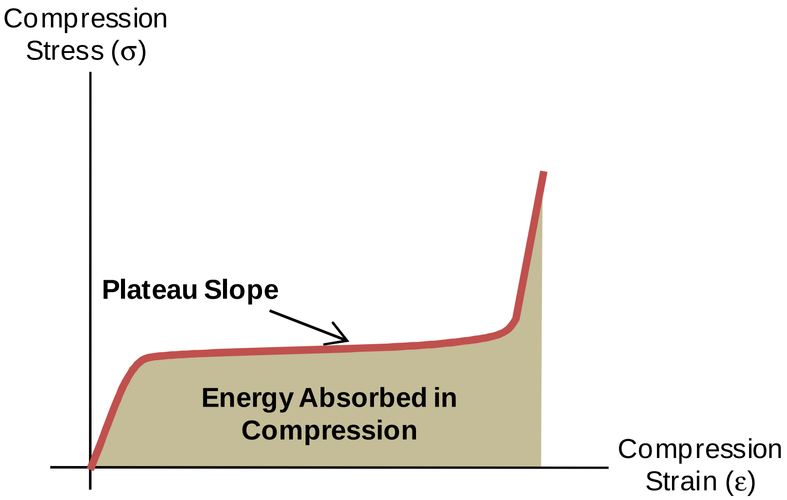

Figure 2. Stress-Strain Load Curve for Idealized Material

Finite Element Modeling of Material

Constitutive Model

The arrestor material was modeled using *MAT_CRUSHABLE_FOAM, as shown below in units of lbf-in-sec (Table 1) (LSTC, 2007). The load curve in such cases was similar to Figure 2 with a strength of 50 psi and a bottoming strain of 0.85. The tensile stress cutoff (TSC) varied depending upon the erosion criterion specified to ensure realistically low energy absorption in tension.

*Table 1. Parameters for *MAT_063 or *MAT_CRUSHABLE_FOAM*

Parameter	Symbol	Description	Value	Unit
MID		Material ID number		
RO	ρ	Density	3.75E-5	lbf-s^2/in^4
E	E	Young’s modulus	2.00E+3	psi
PR	ν	Poisson’s ratio	0.00	
LCID		Load curve ID for nominal stress versus strain		
TSC		Tensile stress cutoff	1 to 50	psi
DAMP		Rate sensitivity via damping coefficient	1.00E-4	

*MAT_ADD_EROSION was used in some versions of the model to allow element failure based upon principal or shear strain criteria, with variation of the strain values as described further below.

Control and Stability

Mesh tangling was problematic due to the highly compressible nature of the material, which routinely underwent 85 to 90% compaction. *CONTACT_INTERIOR was used with a default activation thickness factor F_a = 0.10 to prevent mesh tangling in high compression areas. The interior contact carries a computational penalty, however.

Hourglass energies were problematic in all finite element versions of the models. As such, fully integrated solid elements were implemented (ELFORM = 2,3), but without success. Stability issues plagued versions using these formulations, which were highly prone to simulation crashes under high compaction. The default single-point solid formulation was used for the majority of cases (ELFORM = 1).

Under maximum compression, the element characteristic length decreased by nearly an order of magnitude, causing a proportional decrease in the timestep and increase in overall run time. Mass scaling countermeasures were not considered viable; the tire overruns were to take place at high speed, and mass scaling would have added artificial inertial resistance.

Tire and Arrestor Evaluation

Figure 3 and Figure 4 illustrate the tire rolling through the arrestor and creating a rut of crushed material. The tire in this case represented a Goodyear H44.5x16.5-21 main gear tire for a Boeing 737-800 (Goodyear, 2007). The arrestor bed depth was 20 inches, using 2-inch cubic finite elements.

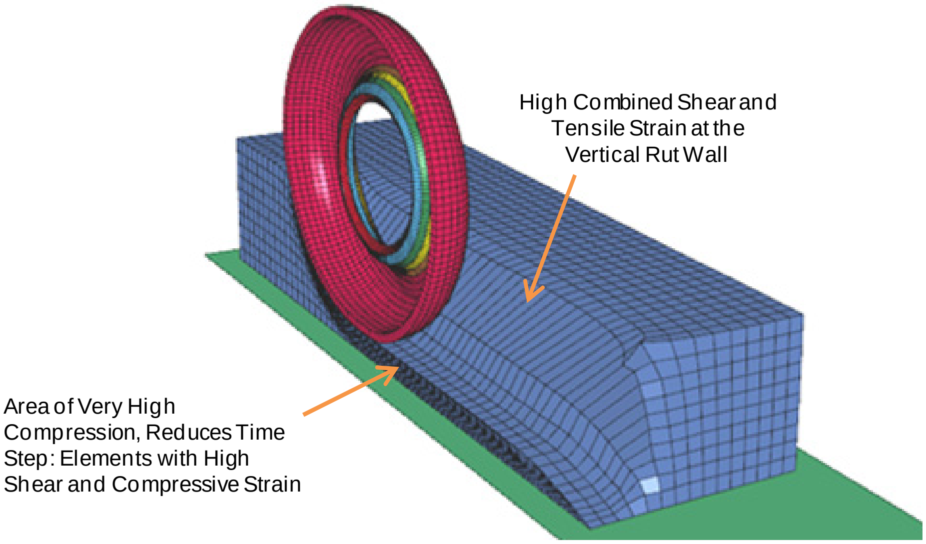

Figure 3. Overview of FEM Arrestor Bed with Tire Overrun (2-inch Elements)

The elements along the vertical sides of the rut deformed substantially, as expected, in both shear and tension (Figure 4). Elements along the bottom of the run underwent high compression. Figure 5 shows a detail of the deformed elements in areas of high compression, where a flattened diamond shape results.

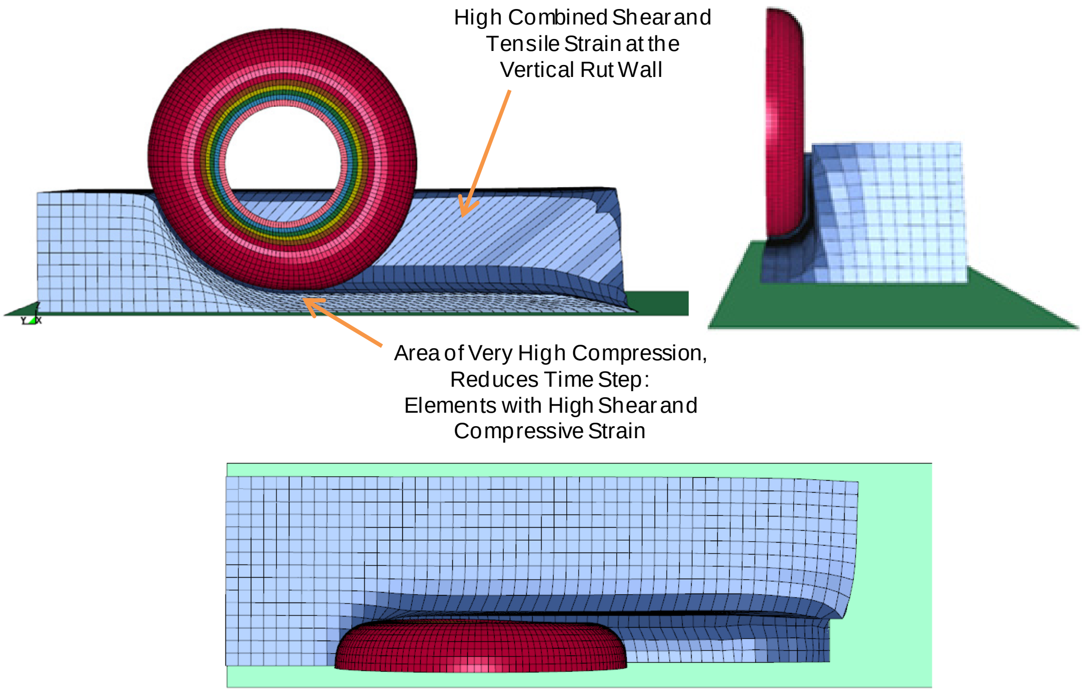

Figure 4. Orthogonal Views of FEM Arrestor Bed with Tire Overrun (2-inch Elements)

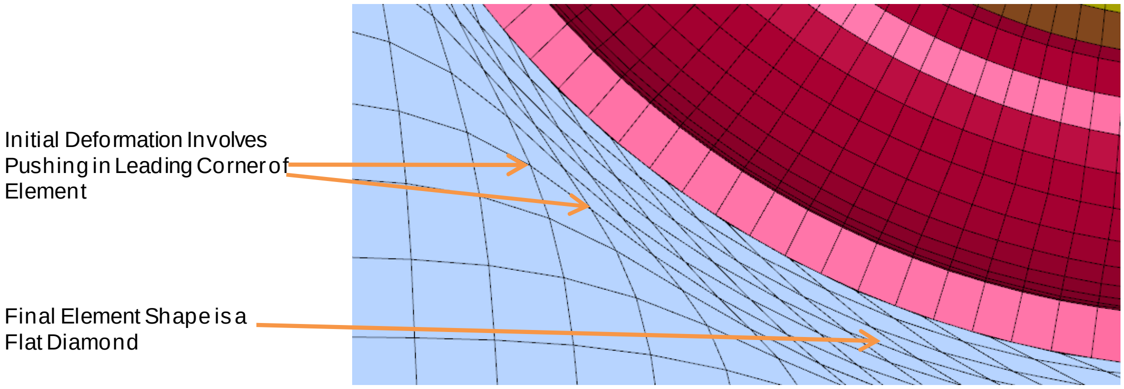

Figure 5. Details of Element Distortion in Combined FEM Arrestor/Tire Model

Hourglass energy was relatively high. All applicable types of hourglass control were implemented in various strengths, but the overall hourglass energy proved irreducible beyond the level of about 14 to 19% of internal energy.

The deformation sequence of the elements precipitated problems when attempting to implement element erosion. Principal strain and shear strain criteria were both used with mixed results. Problematically, the deformation sequence triggered erosion relatively early with either criterion, before the elements had undergone substantial compression or absorbed much energy.

These issues were exacerbated by cases involving deep material (Figure 6). In actual overruns, the upper part of the material would break off and form furrows. Erosion criteria with higher strain limits, as required for the elements at the rut bottom, allowed the upper elements to over-stretch and form tunnels. Lower strain limits created more realistic failure in the upper area, but caused premature erosion at the bottom of the rut and cascading material failure beneath the tire.

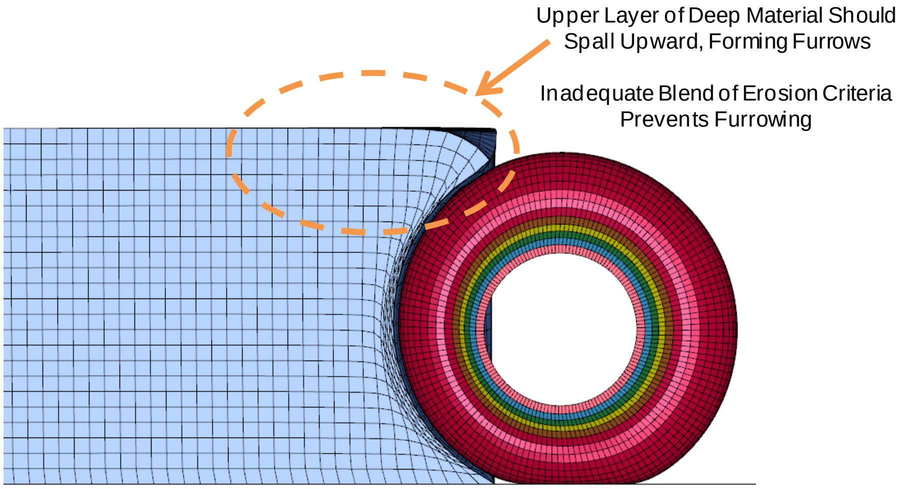

Figure 6. Problematic Furrowing Loading Mode in Deep Material for FEM Arrestor/Tire Model

Summary of FEM Model Findings

Overall, the FEM model for the material had several shortcomings:

- The tire overrun produced a shearing distortion of the arrestor elements;
- Element erosion did not adequately resolve the distortion;
- Hourglass energy remained high even with best-case settings;
- The 85% compression of the material reduced the timestep by nearly an order of magnitude; and
- The FEM approach was not readily adaptable for modeling the plowing action of a tire in deep material.

Smoothed Particle Hydrodynamics Modeling of Material

The Smoothed Particle Hydrodynamics (SPH) method was applied to the arrestor model in lieu of finite elements. The meshless approach of SPH proved more robust for this high compaction and high dislocation application. The particles of SPH are inherently dissociative, which better matches the actual crushable foam material at a behavioral level. The constitutive model used essentially the same values as given in Table 1.

Control and Stability

The SPH formulation in LS-DYNA is controlled through three keywords (LSTC, 2007):

- *CONTROL_SPH
- *SECTION_SPH
- *BOUNDARY_SPH_SYMMETRY_PLANE

Default properties were used for most parameters, including the particle formulation (FORM=0). However, the number of cycles between bucket sorts (NCBS) was set to 10 to improve computational time efficiency by 20%.

Tire and Arrestor Evaluation

The SPH arrestor bed performed well and seemed suited to the modes of deformation experienced. The tire cut a clean rut through the material, leaving a crisp vertical rut wall, while compressing the bottom material. Since the particles could undergo dislocations and separations, erosion was not necessary (nor possible). This provided superior performance along areas of shear failure, such as the rut side-wall.

The timestep remained constant throughout the simulation, which was an advantage not shared by the finite element versions of the model.

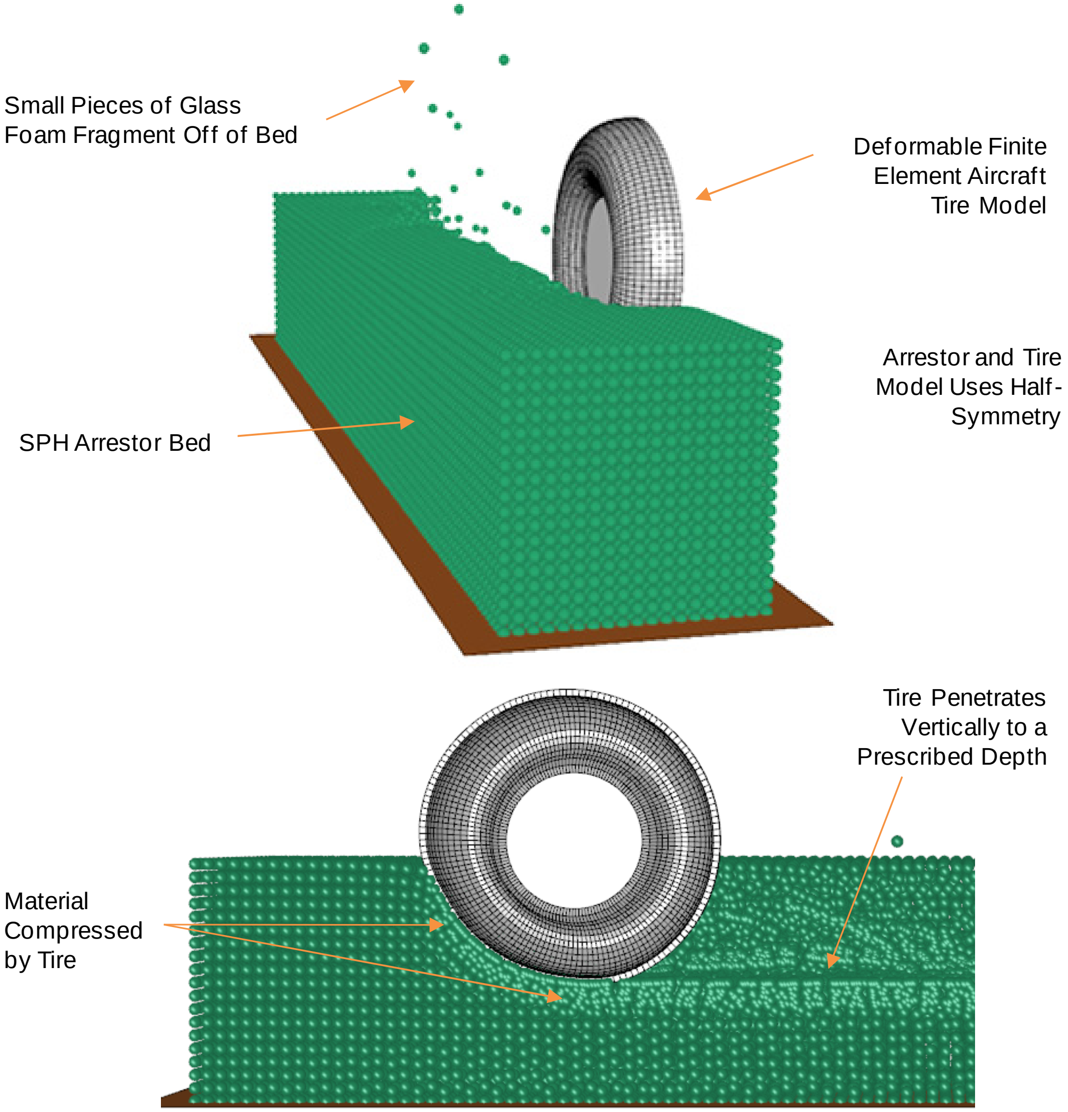

Figure 7. Model of Combined Tire & Crushable Foam Arrestor System

Summary of SPH Model Findings

The SPH formulation proved itself to be a robust, durable representation of the crushable material, including:

- Natural dislocation and separation of the material without mass/volume losses due to erosion;
- Constant timestep; and
- Good shear failure performance at rut side walls.

Error Convergence Comparison of Methods

Qualitatively, the SPH method seemed to provide a superior fit for the problem at hand. A three-stage error convergence study was undertaken to compare it side-by-side with the FEM version of the material, in order to determine if SPH would also provide accurate quantitative predictions. The convergence study was conducted in one-, two-, and three-dimensional forms.

The FEM and SPH methods did not carry equivalent assumptions of convergence; it has been noted that SPH lacks a rigorous convergence and refinement theory (Li, et al., 2007). As such, newer FEM-specific error estimation methods have been neglected in favor of a simpler analysis of measured functionals (Babuska, et al., 2001). Various performance metrics (energy absorption rate, vertical load, and drag load) were measured at multiple mesh discretizations. Power-function convergence trends per Richardson's Extrapolation method were assumed *a priori*, and later confirmed to be uniformly applicable (eq 1) (Kardestuncer, 1987).

$$e_{\phi}(h) = \phi - \phi_{ext} = K \cdot h^{p} \tag{1}$$

Where:

$e_{\phi} = error\ in\ functional$

$\phi = functional\ value\ for\ a\ particular\ mesh$

$\phi_{ext} = extrapolated,\ converged\ functional\ value$

$K = constant$

$h = characteristic\ mesh\ size$
$p = order\ of\ convergence$

Convergence for each case was analyzed using one of two methods:

- Grid Convergence Index (GCI) (Celik, Undated); this method worked well for three discretizations only and for cases where the scatter in the convergence trend was minimal.

- Power-function regression fitting; this method worked better for cases with more data scatter and was required if more than three mesh sizes were to be analyzed.

In the convergence study that follows, uniform mesh refinement is employed. The FEM approach could feasibly be improved using adaptive remeshing, which would improve the per-element Jacobian in areas of distortion. However, in LS-DYNA, adaptive remeshing for solids is only available for tetrahedrons using essentially incompressible materials. Hence, it is not applicable to this LS-DYNA modeling problem.

1-D Convergence Study

The one-dimensional model simulated a platen compression test (zero Poisson ratio). The specimen had dimensions of 12”x12”x24”, which was representative of a nominal 24-inch deep arrestor bed (Figure 8). Three mesh densities were used, with elements/particles sized at h = 4, 2, and 1 inch.

The specimen was compressed uniaxially to a principal strain of ε_1 = 85%. The boundary conditions included symmetry definitions along the vertical faces of the specimens to ensure one-dimensional behavior.

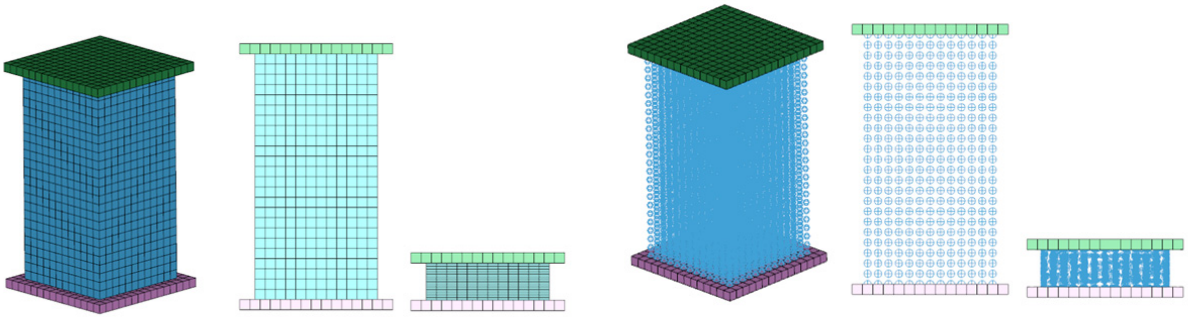

Figure 8. Uniaxial FEM (left) and SPH (right) Compression Specimens

Figure 9 shows the performance of the FEM and SPH models. The force plots clearly show that the FEM version has much higher accuracy, closely following the baseline plot of the defined material load curve.

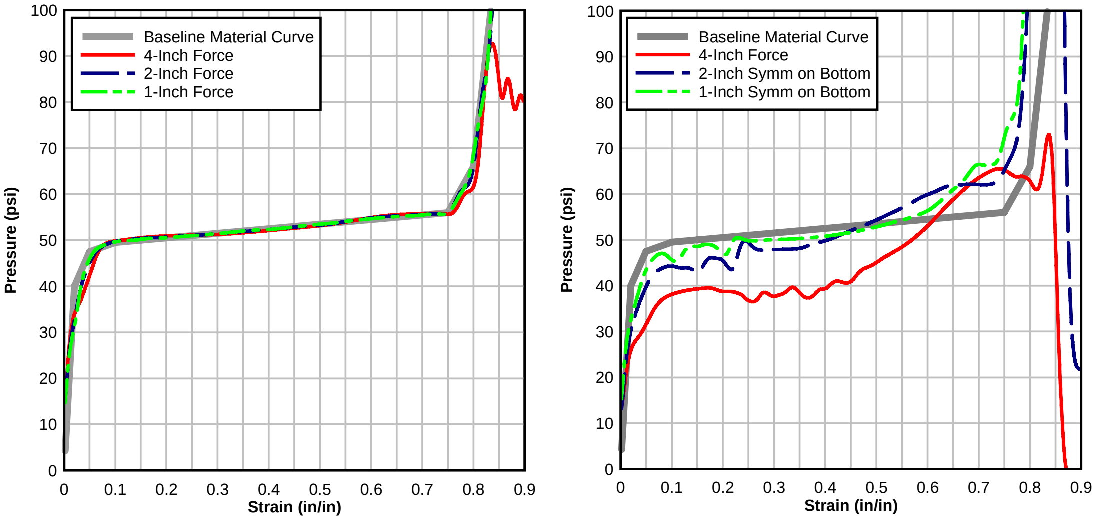

Figure 9. 1-D FEM (left) and SPH (right) Compression Force Performance

Table 2 summarizes the convergence of the RMS (root-mean-squared) error for the compressive energy absorption as compared with the integrated material stress-strain curve. Convergence was assessed using via regression analysis. Both the FEM and SPH cases had high convergence rates, with orders *p* of 4.165 and 3.293, respectively.

A glance at the final converged values for the energy RMSE (ϕ_{ext}) underscores the superiority of the FEM method over SPH, since FEM converges to 0.73% RMSE and SPH converges to 3.78%. This apparent superiority is fleeting, however, as the addition of more dimensions makes clear in subsequent sections.

Table 2. Convergence Summary for 1-D Case, Regression Power-Function Fit

			Absorbed Energy RMSE
FEM	P	Order of Convergence	4.165
	ϕ_{ext}	Converged Value	0.73%
	R^2	Fit Quality	0.999
SPH	P	Order of Convergence	3.293
	ϕ_{ext}	Converged Value	3.78%
	R^2	Fit Quality	1.000

2-D Convergence Study

The two-dimensional case modeled a planar version of a rigid tire form rolling through the crushable material (Figure 10 and **Error! Reference source not found.**). Three mesh densities were used, with elements/particles sized at h = 4, 2, and 1 inch.

The bed was 24 inches deep and 200 inches long; the rigid roller diameter was 44.5 inches. The roller followed a constrained displacement path to a penetration depth of -16.0 inches while travelling forward at 1,418 in/s (70 knots).

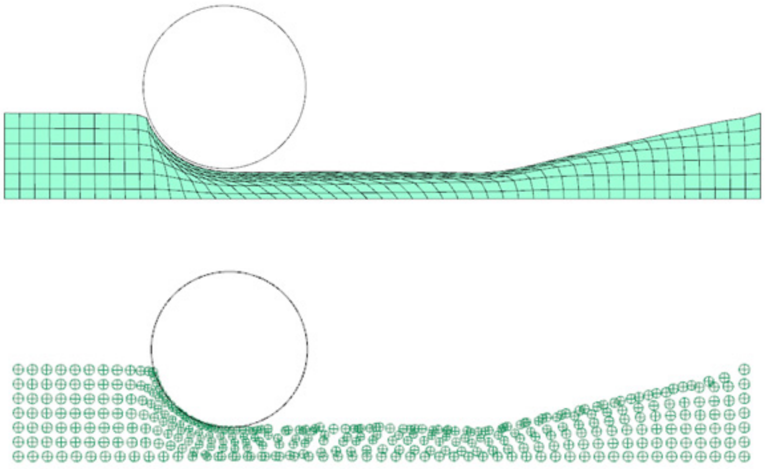

Figure 10. 2-D FEM (top) and SPH (bottom) Rigid Roller Models, 4-inch Elements

Table 3 summarizes selected GCI tabular data, including the GCI value, the asymptotic value, and the order of the convergence. The hourglass energy for the FEM version at the predicted convergence was nominally 17% of the internal energy value. Meanwhile, the SPH method showed comparable convergence levels and no hourglass energy. Overall, the SPH method showed GCI values on par with the FEM orthogonal approach.

Table 3. Convergence Summary for 2-D Case, Grid Convergence Index Method

			Vertical Load	Drag Load	Internal Energy	Hourglass Energy	Hourglass Percentage of Internal
FEM	P	Order of Convergence	1.04	1.42	1.04	1.84	
	ϕ_{ext}	Converged Value	875 lbf	(1,091) lbf	110,195 lbf-in	18,711 lbf-in	17.0%
	GCI	Convergence Quality	9.8%	3.8%	2.0%	11.8%	
	$e_{ext}^{1"}$	Error of Finest Mesh	8.5%	3.1%	1.6%	10.4%	
SPH	P	Order of Convergence	1.01	1.02	1.28		
	ϕ_{ext}	Converged Value	845 lbf	(1,117) lbf	122,850 lbf-in		
	GCI	Convergence Quality	5.0%	5.5%	2.5%		
	$e_{ext}^{1"}$	Error of Finest Mesh	4.2%	4.6%	2.9%		

3-D Convergence Study

The three-dimensional study featured a deformable B737-800 main gear tire (Goodyear H44.5x16.5-21) that was rolled through an arrestor bed strip. The bed was 24 inches deep, 200 inches long, and 12 inches wide, with a symmetry plane defined down the centerline of the tire (Figure 11). Just as in the two-dimensional version, the tire followed a constrained displacement path to a penetration depth of 16.0 inches while travelling forward at 1,418 in/s (70 knots). The bottom and outside nodes of the arrestor were constrained for the FEM method, while the SPH version used partial constraints and an outside SPH symmetry plane.

Three discretization densities were originally defined, with elements/particles sized at h = 3, 2, and 1 inch (Figure 11). Additional meshes between these three primary values were also run for the different cases.

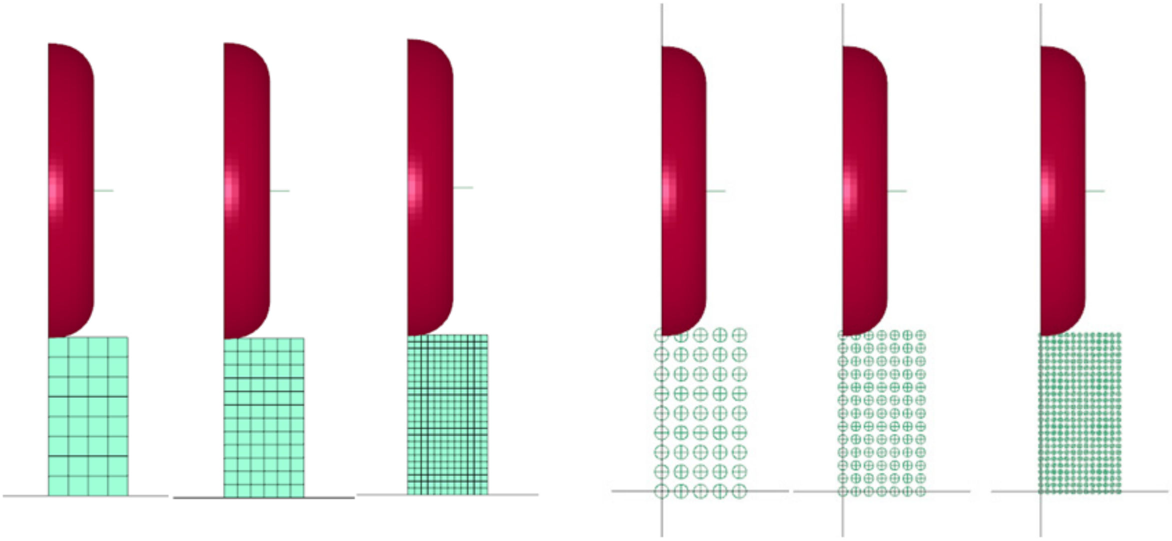

Figure 11. 3-D FEM (left) and SPH (right) Models with 3-, 2-, and 1-Inch Element Sizes

Table 4 summarizes the regression convergence results. As shown, the hourglass energy remains too high for the FEM method: 19% even at a 1-inch mesh density. The drag force for SPH was unusual among the functionals measured, having a low R^2 value due to a very flat trend combined with scatter in the data; the drag force was so consistent across the different meshes that the only significant variations were due to noise (Figure 14). As the table shows for the p values, the SPH version converges at least twice as quickly as the FEM version. Further, the SPH version has nearly an order of magnitude less error than the FEM version for the 1-inch mesh density.

Table 4. Method Convergence Summary, Regression Power-Function Fit

			Vertical Force	**Drag Force**	**Energy Absorption**	**Hourglass Energy**	**Hourglass Percentage of Internal**
FEM	P	Order of Convergence	1.472	1.162	1.000	1.828	
	ϕ_{ext}	Converged Value	10,730 lbf	8,144 lbf	7,591 lbf-in/in	1,548 lbf-in/in	19.4%
	R^2	Fit Quality	0.999	0.999	0.995	0.999	
	$e_{ext}^{1''}$	Error of Finest Mesh	15.3%	23.4%	9.4%	27.6%	
SPH	P	Order of Convergence	3.331	6.902	2.263		
	ϕ_{ext}	Converged Value	10,400 lbf	10,030 lbf	7,996 lbf-in/in		0%
	R^2	Fit Quality	0.993	0.786	0.998		
	$e_{ext}^{1''}$	Error of Finest Mesh	0.3%	1.2%	1.5%		

Figure 12 through Figure 14 illustrate several examples of measured functional data and their regression curve fits. In these figures, the SPH version follows the power-law convergence form more consistently than the FEM method, converges more quickly, and has less error for any given mesh density.

In Figure 14, it is clear that the FEM and SPH methods converge to different values for the drag force. In assessing this discrepancy, the SPH method was deemed more trustworthy for several reasons:

- The SPH models and measured values were more stable;
- The FEM method, as an alternative, presented a very low order of convergence ($p = 1.16$);
- The FEM method still retained substantial hourglass energy
- A separate punch test model (not shown) revealed that SPH predicted resulting shear force along failure surfaces better than the FEM, which is present along the rut side wall of this model.

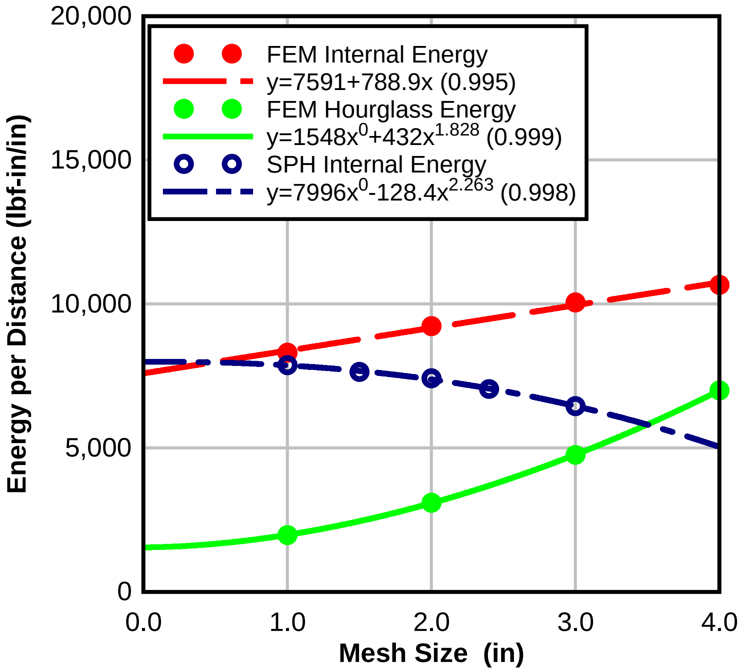

Figure 12. 3-D Convergence of Internal and Hourglass Energy

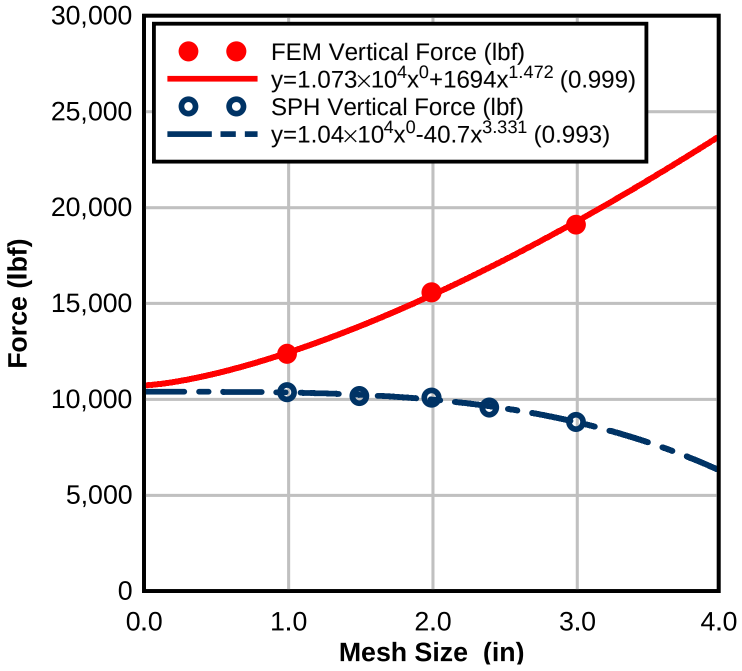

Figure 13. 3-D Convergence of Vertical Force

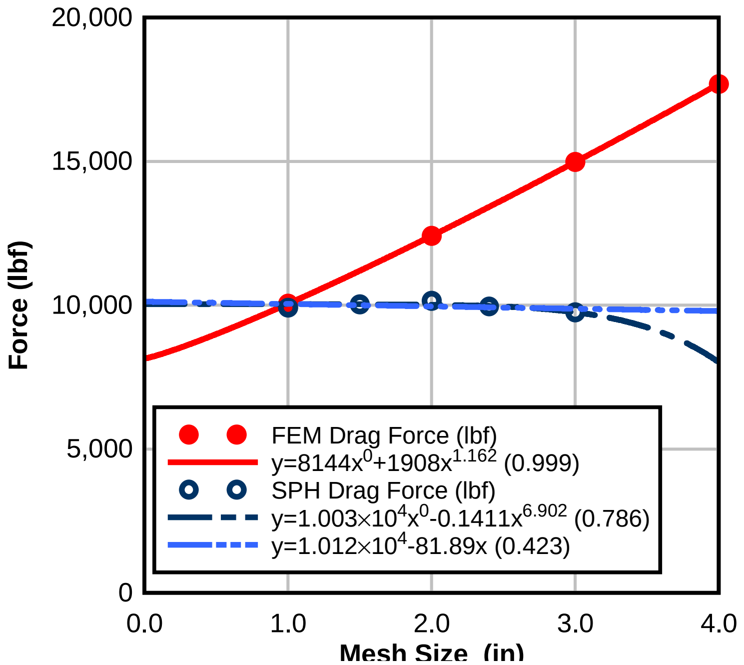

Figure 14. 3-D Convergence of Drag Force

Conclusions

For the modeling of high-compaction foam materials as used in aircraft overrun applications, the finite element method proved to have several shortcomings that were difficult to resolve. The nature of the crushable foam featured cracking and dislocations preceding full compaction, which rendered erosion criteria ineffective at capturing the overall behavior at low, medium and upper areas through the arrestor bed thickness.

The smoothed particle hydrodynamics (SPH) formulation was found to provide better results due to its inherently meshless dissociative nature, which more closely reflected the actual material's behavior during an overrun. Because the SPH method lacks the foundational convergence theory inherent to the FEM approach, great care was taken to ensure that the SPH method was sufficiently accurate for the modeling effort. A three-stage convergence study examined the two methods in one-, two-, and three-dimensional forms.

In cases where the crushable foam material underwent fairly orthogonal compression, as in the uniaxial model, the FEM version had superior accuracy and computational efficiency. Substantial hourglass effects appeared in the FEM version for the two-dimensional case, however, and the SPH method drew even with the FEM method in terms of convergence performance. In three dimensions, SPH took a strong lead over FEM with:

- No hourglassing;
- No element skewing;
- Convergence rates of double or higher;

- Error levels nearly an order of magnitude less;
- Constant timestep regardless of compaction; and
- Similar overall computational efficiency.

Therefore, SPH was selected as the LS-DYNA modeling method of choice for the larger research effort, where it was incorporated into a broad set of parametric investigations using LS-OPT. The robustness of the SPH model allowed a broad range of material parameters to be explored with stability surpassing the more fickle FEM version of the model.

References

[1]**Babuska, Ivo and Strouboulis, Theofanis. 2001.** *The Finite Element Method and its Reliability.* Oxford : Oxford University Press, 2001.

[2]**Barsotti, Matthew A. 2008.** *Optimization of a Passive Aircraft Arrestor with a Depth-Varying Crushable Material Using a Smoothed Particle Hydrodynamics (SPH) Model.* University of Texas at San Antonio. Austin, TX : UMI, 2008. Graduate Thesis.

[3]**Barsotti, Matthew, Puryear, John and Stevens, David. 2009.** *Developing Improved Civil Aircraft Arresting Systems.* Washington, DC : Transportation Research Board, Airport Cooperative Research Program, 2009. Report 29.

[4]**Celik, Ismail.** *Procedure for Estimation and Reporting of Discretization Error in CFD Applications.* Mechanical and Aerospace Engineering Department, West Virginia University. Morgantown, WV : West Virginia University.

[5]**FAA. 2005.** *AC 150-5220-22a: Engineered Materials Arresting Systems (EMAS) for Aircraft Overruns.* s.l. : Federal Aviation Administration, 2005.

[6]**Goodyear. 2007.** *Aircraft Tire Data Book.* Akron, OH : Goodyear Tire & Rubber Company, 2007.

[7]**Kardestuncer, Hayrettin, [ed.]. 1987.** *Finite Element Handbook.* New York : McGraw-Hill Book Company, 1987.

[8]**Li, Shaofan and Liu, Wing Kam. 2007.** Smoothed Particle Hydrodynamics (SPH). *Meshfree Particle Methods.* s.l. : Springer Berlin Heidelberg, 2007, pp. 25-67.

[9]**LSTC. 2007.** *LS-DYNA Keyword User's Manual.* v971. Livermore : Livermore Software Technology Corporation, 2007. p. 18.